scientific reports

Check for updates

OPEN

Pressure and temperature predictions of Al_2O_3/water nanofluid flow in a porous pipe for different nanoparticles volume fractions: combination of CFD and ACOFIS

Meisam Babanezhad[1,2,3], Iman Behroyan[4,5], Azam Marjani[6,7]✉ & Saeed Shirazian[8]

Artificial intelligence (AI) techniques have illustrated significant roles in finding general patterns of CFD (Computational fluid dynamics) results. This study is conducted to develop combination of the ant colony optimization (ACO) algorithm with the fuzzy inference system (ACOFIS) for learning the CFD results of a physical case study. This binary join of the ACOFIS and CFD was used for pressure and temperature predictions of Al_2O_3/water nanofluid flow in a heated porous pipe. The intelligence of ACOFIS is investigated for different input numbers and pheromone effects, as the ant colony tuning parameter. The results showed that the intelligence of the ACOFIS could be found for three inputs (x and y nodes coordinates and nanoparticles fraction) and the pheromone effect of 0.1. At the system intelligence, the ACOFIS could predict the pressure and temperature of the nanofluid on any values of the nanoparticles fraction between 0.5 and 2%. Comparing the ANFIS and the ACOFIS, it was shown that both methods could reach the same accuracy in predictions of the nanofluid pressure and temperature. The root mean square error (RMSE) of the ACOFIS (~ 1.3) was a little more than that of the ANFIS (~ 0.03), while the total process time of the ANFIS (~ 213 s) was a bit more than that of the ACOFIS (~ 198 s). The AI algorithms process time (less than 4 min) shows their ability in the reduction of CFD modeling calculations and expenses.

Nanofluids possess an increasing utilization in thermal engineering industries in order to improve the heat transfer efficiency and reduce heat loss and energy costs[1–6]. In these novel heat transfer fluids (HTFs), the well-known Brownian movement of the nanoparticles (NPs) in the medium, known as the important parameter, influences the nanofluids' heat transfer rate[7]. Using porous media could also increase heat transfer rates considerably. The porous matrix causes more heat transfer area, higher thermal conductivity, and more mixing effect. So, it is a promising research area to use both nanofluid and porous media for different kinds of application such as heat exchangers (e.g. shell and tube type) due to the synergistic effect of nanofluids and porous media[8,9].

Some studies have been focused on the nanofluids' heat transfer in porous structures[10–12]. Nazari et al.[10] experimentally analyzed heat transfer of water/CuO nanofluid (NF) in foam tubes with various types of configurations, and assessed the heat transfer rates[13]. It was revealed by them the improvements of heat transfer by the dispersion of the NPs into the base fluids for metal and helical foam tubes, comparing to the straight tube. In a study[12], the development of convection for alumina/water NF was considered in a tube occupied by an

[1]Institute of Research and Development, Duy Tan University, Da Nang 550000, Viet Nam. [2]Faculty of Electrical-Electronic Engineering, Duy Tan University, Da Nang 550000, Viet Nam. [3]Department of Artificial Intelligence, Shunderman Industrial Strategy Co., Tehran, Iran. [4]Faculty of Mechanical and Energy Engineering, Shahid Beheshti University, Tehran, Iran. [5]Department of Computational Fluid Dynamics, Shunderman Industrial Strategy Co., Tehran, Iran. [6]Department for Management of Science and Technology Development, Ton Duc Thang University, Ho Chi Minh City, Viet Nam. [7]Faculty of Applied Sciences, Ton Duc Thang University, Ho Chi Minh City, Viet Nam. [8]Laboratory of Computational Modeling of Drugs, South Ural State University, 76 Lenin prospekt, 454080 Chelyabinsk, Russia. ✉email: azam.marjani@tdtu.edu.vn

aluminum metal foam. It was reported the heat transfer enhancement is caused by the increase of the nanofluid concentration and the Reynolds number as well.

As discussed above, a few studies have considered the potential of the application of nanofluids in porous ducts. So, this concept is still attractive for researchers in many aspects, specifically for process engineers to develop novel HTFs for industrial applications. Besides, the computational fluid dynamics (CFD) approach is a perfect and versatile tool for the predictions and simulations of thermal and hydrodynamic parameters of fluid flows in different regimes and geometries[14]. CFD modeling requires to solve many calculations on the system nodes to obtain the desired distributions, such as pressure and velocity. However, these calculations could be complex for 3-dimension analysis, turbulent flows, complex geometries, large scale cases, multi-phase flows, etc. For instance, the CFD modeling has its own difficulties and challenges for the evaluation of nanofluids flow characteristics in porous media. Changing in the nanoparticles concentrations is caused to the changes in thermo-physical properties of the nanofluids which need to be considered in the CFD simulations. Hence, a new simulation strategy is required for the new nanoparticles concentrations that can obviate the need for expensive and tedious CFD calculations. From the engineering point of view, pressure and temperature could be the important parameters of nanofluid flow in porous media which should be precisely predicted by theoretical methods. A supplementary method is needed to optimize the CFD approach and make it faster. Artificial intelligence (AI) algorithms have the potential in finding the pattern of simulation data. AI algorithms could learn the CFD results for several specific conditions (e.g. specific positions, times, properties, boundary conditions, etc.), find the general pattern of data, and predict the targeted variables for the other conditions without any further computational expenses. The machine learning of the CFD results was used for the first time by references[15–22]. The researchers used the fuzzy inference system (FIS) with the adaptive network (AN) algorithm for the training process. There are a number of other trainers such as genetic algorithm (GA), ant colony optimization (ACO), neural network (NN), etc. that are available and could be used with integration with FIS. Every AI algorithm that possesses the highest level of accuracy would be called the best intelligent condition. There are several parameters, specifically for each AI algorithm, defining the best intelligence condition. These parameters could be changeable from one CFD case study to another one. The details of the artificial intelligence algorithm and also the effects of the parameters are absent in these studies. Additionally, the extra investigations are required to show the contribution of other trainers like ant colony optimization with the FIS for helping the CFD.

This study tries to do machine learning of the CFD results of a nanofluid flow in a porous media for some specific nanoparticle concentrations. The ant colony optimization-based fuzzy inference system (ACOFIS) is developed, for the first time, for this purpose. After obtaining the best intelligence, the pressure and temperature can be predicted by the ACOFIS for any other values of the nanoparticles concentrations without any other CDF modeling. The computational times of the ACOFIS are presented for such a case as feedback for facilitating the CFD method. The general parameter of input number and the specific one, the pheromone effect related to ant colony optimization, are considered for sensitivity tests of the best intelligence condition.

Methodology

Computational fluid dynamics. A cylindrical duct with a length (L) of 1.0 m completely occupied with a porous medium was considered as the geometrical configuration, in which the porous medium is saturated with a circular section with the diameter of 0.01 m (D) and a single phase. The single-phase model with a mixture behaving like a single-phase fluid hypothetically was taken into account in this work. The nanofluid within the single-phase model is considered as a normal fluid, but with improved features owing to the presence of nanoparticles in the system.

The mathematical explanation of single-phase leading equations is represented as follows[23–26].

Continuity equation:

$$\nabla \cdot \left(\rho_{eff} V\right) = 0 \tag{1}$$

Momentum equation:

$$\frac{1}{\varepsilon^2}\nabla \cdot \left(\rho_{eff}\vec{V}\vec{V}\right) = -\nabla p + \frac{1}{\varepsilon}\nabla\left[\mu_{eff}^{e}\left(\nabla\vec{V} + \left(\nabla\vec{V}\right)^{T}\right)\right] - \frac{\mu_{eff}}{K}\vec{V} - \frac{\varepsilon C_d \rho_{eff}}{\sqrt{K}}|V|\vec{V} \tag{2}$$

Energy equation:

$$\nabla \cdot \left(\rho_{eff} V C_{p.eff} T\right) = \nabla \cdot \left(\varepsilon k_{eff}\nabla T - \varepsilon\left(\rho C_p\right)_{eff}\overline{VT}\right) \tag{3}$$

The parameters of porous media such as porosity ε, inertia coefficient C_d and permeability K are reported in references[27–30].

$$K = 0.00073 d_{pore}^2 (1-\varepsilon)^{-0.224}\left(\frac{d_{cell}}{d_{pore}}\right)^{-1.11} \tag{4}$$

$$C_d = 0.00212(1-\varepsilon)^{-0.132}\left(\frac{d_{cell}}{d_{pore}}\right)^{-1.63} \tag{5}$$

$$d_{pore} = 0.0254(m)/10(PPI) \tag{6}$$

Properties	Equation
Density[23]	$\rho_{eff} = (1-\varphi)\rho_f + \varphi\rho_p$
Heat capacity[23]	$c_{p,eff} = \frac{(1-\varphi)(\rho c_p)_f + \varphi(\rho c_p)_p}{(1-\varphi)\rho_f + \varphi\rho_p}$
Viscosity[32]	$\mu_{eff} = \left(1 + \frac{\rho_{np} v_B d_p^2}{72C\delta}\right)\mu_f$ $v_B = \frac{1}{d_p}\sqrt[3]{\frac{18K_B T}{\pi\rho_{np} d_p}}$ $\delta = \sqrt[3]{\frac{\pi d_p}{6\phi}}$
Thermal conductivity[31]	$k_{nf}/k_{bf} = 1 + 64.7(\phi)^{0.7460}\left(\frac{d_{bf}}{d_p}\right)^{0.3690}\left(\frac{k_{bf}}{k_p}\right)^{0.7476} Pr^{0.9955} Re_{np}^{1.2321}$ $Re_{np} = \frac{\rho_{bf} K_B T}{3\pi\mu_{bf}^2 \lambda}$

Table 1. Al_2O_3/water properties.

Study	Fluid	Tube type	Re	Nu
Fotukian and Esfahany[35]	0.054% Al_2O_3/water	Simple tube	9,950	82.95
	0.14% Al_2O_3/water	Simple tube	7,084.23	67.07
	0.14% Al_2O_3/water	Simple tube	10,799.1	86.13
Present study	0.3% Al_2O_3/water	Simple tube	10,000	85.86
	2% Al_2O_3/water	Simple tube	10,000	99.13
	2% Al_2O_3/water	Porous tube	10,000	306.27

Table 2. Nusselt number calculation (CFD and experiment comparison).

$$d_{cell} = 1.18 d_{pore}\sqrt{\frac{1-\varepsilon}{3\pi}}\left(\frac{1}{1-e^{\frac{-(1-\varepsilon)}{0.04}}}\right) \tag{7}$$

Effective thermal conductivity is influenced by nanofluid thermal conductivity and the copper porous conductivity and is given as follows[27,30]:

$$k_{eff} = (1-\varepsilon)k_{porous} + \varepsilon k_{nf} \tag{8}$$

The effective thermophysical properties of the nanofluid are collected in Table 1. Considering the effect of Brownian phenomenon, Chon et al.[31] correlation is adopted for the calculation of thermal conductivity, while the correlation suggested by Masoumi et al.[32] is employed for estimating the fluid viscosity. So, for using such temperature-dependent correlations of conductivity and viscosity, User Defined Function (UDF) codes have been developed and added to the ANSYS-FLUENT CFD codes.

The $k-\varepsilon$ turbulence model to calculate the turbulent eddy viscosity, its energy dissipation rate (ε), and the turbulent kinetic energy (k) are based on the literature[23,33,34]:

$$\nabla\cdot(\rho_{eff} kV) = \nabla\cdot\left[\left(\frac{\mu_t}{\sigma_k}\right)\nabla(k)\right] + G_k - \rho_{eff}\varepsilon \tag{9}$$

$$\nabla\cdot(\rho_{eff}\varepsilon V) = \nabla\cdot\left[\frac{\mu_t}{\sigma_\varepsilon}\nabla\varepsilon\right] + \frac{\varepsilon}{k}(C_{1\varepsilon}G_k - C_{2\varepsilon}\rho_{eff}\varepsilon) \tag{10}$$

$$G_k = \mu_t(\nabla V + (\nabla V)^T),\ \mu_t = \rho_{eff} C_\mu \frac{k^2}{\varepsilon} \tag{11}$$

$$C_\mu = 0.09, \sigma_k = 1.00, \sigma_\varepsilon = 1.30, C_{1\varepsilon} = 1.44, C_{2\varepsilon} = 1.92$$

CFD grid test and validation. The mesh dependency test has been carried out for two different grid arrangements (i.e. 107,400 nodes, and 161,100 nodes). According to the CFD results and testing both mesh sizes, the relative temperature and velocity differences were less than 0.05%. So, the first mesh size was selected for the calculations due to less computational expenses and shorter solution time.

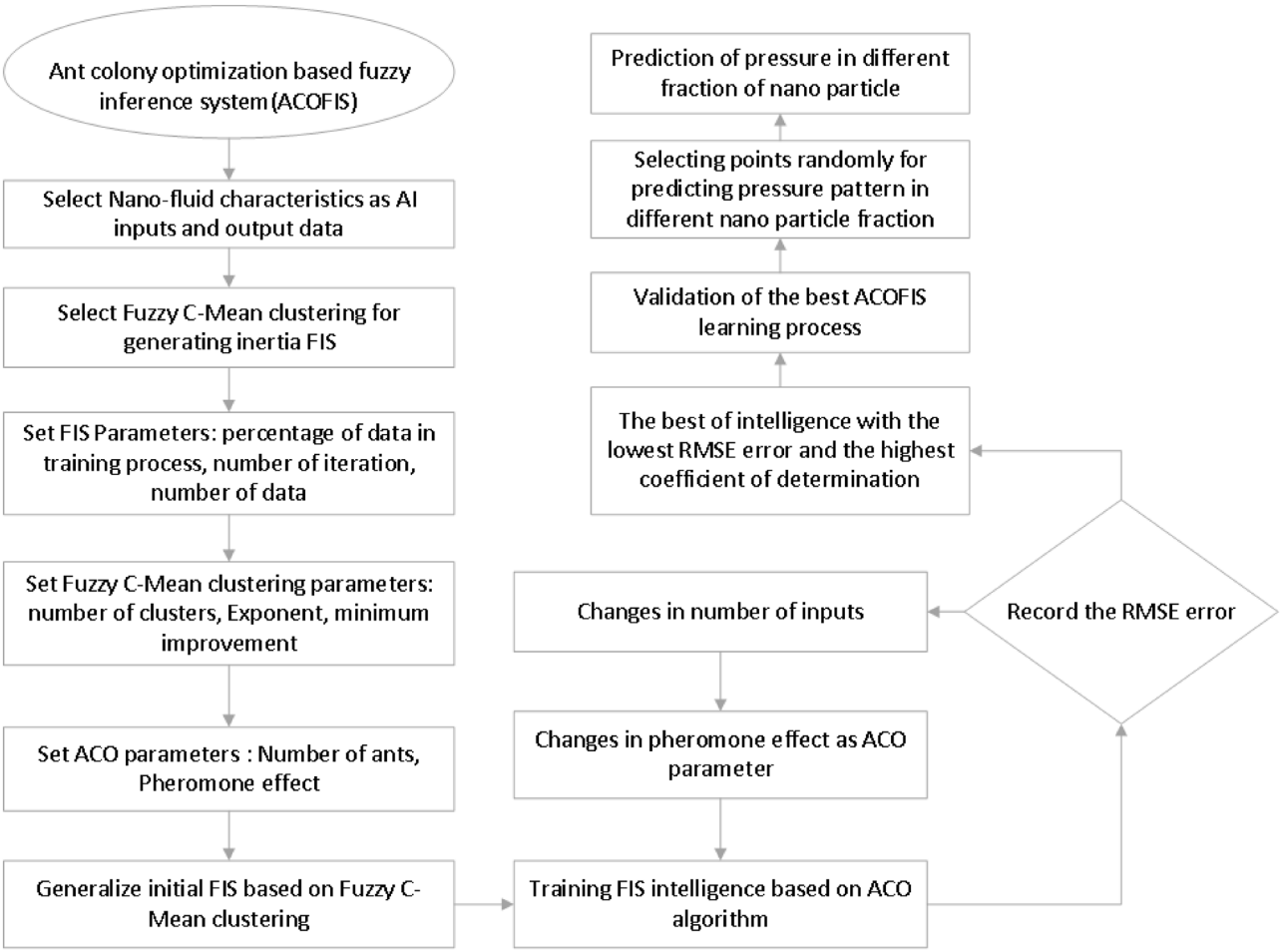

Figure 1. Schematics of combination of ant colony algorithm with fuzzy system.

For verifying the CFD outputs, calculated Nusselt numbers (Nu) are compared with those measured data of Fotukian and Esfahany[35] investigations. According to Table 2, the CFD results for the simple tube (without porous) are the same as those of the experiment. Inserting the porous material inside the pipe, the Nu becomes threefold.

Ant colony optimization (ACO). Ant System (AS) is the first ant colony optimization method aimed at finding the shortest routes for linking some cities[36]. The same concept is used in development of ACO algorithm[37]. The colony's experience is reflected by the pheromone factor, however, the heuristic factor deals with the interest in choosing a component based on an objective function[38]. These parameters are weighted through α and β as[38,39]:

$$P_{ij}^{k} = \frac{[\tau_{ij}]^{\alpha}[\eta_{ij}]^{\beta}}{\sum_{l} \in N_i^k [\tau_{il}]^{\alpha}[\eta_{il}]^{\beta}}, \quad if\ j \in N_i^k \tag{12}$$

Pheromone trails are updated when all of the ants create their tours[38,39]:

$$\tau_{ij} \leftarrow (1-\rho)\tau_{ij}, \forall (i,j) \in L \tag{13}$$

Furthermore, by leaving pheromone over the arcs crossed by the ants in their pathway and by the superior the tour, the higher the quantity of pheromone will be received for the arcs[38,39]:

$$\begin{aligned} \tau_{ij} &\leftarrow \tau_{ij} + \sum_{k=1}^{n} \Delta\tau_{ij}^{k}, \forall (i,j) \in L \\ \Delta\tau_{ij}^{k} &= \begin{cases} \frac{1}{C^k}, & if arc(i,j)\, belongs to T^k; \\ 0, & otherwise; \end{cases} \end{aligned} \tag{14}$$

The first enhancement of initial ant system was known as the elitist approach for AS. It deals with providing robust additional reinforcement for the arcs related to the best tour found since starting the method[38–40]:

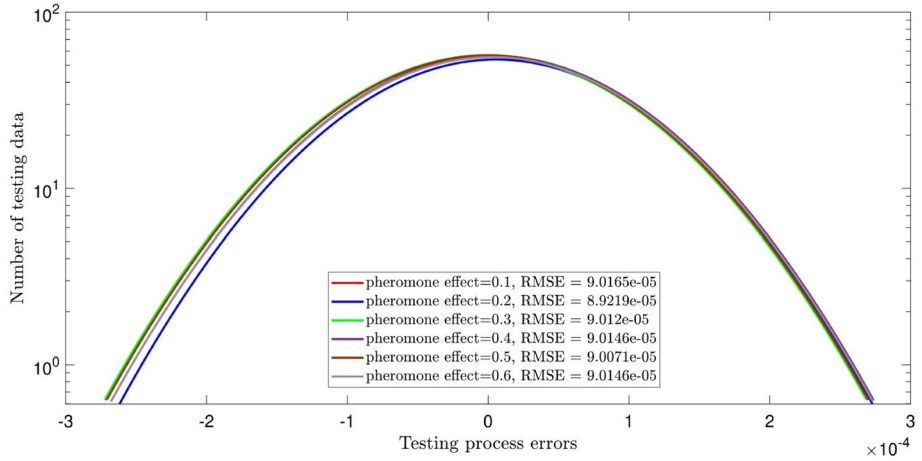

Figure 2. ACOFIS learning processes using two inputs and diversity of pheromone effect.

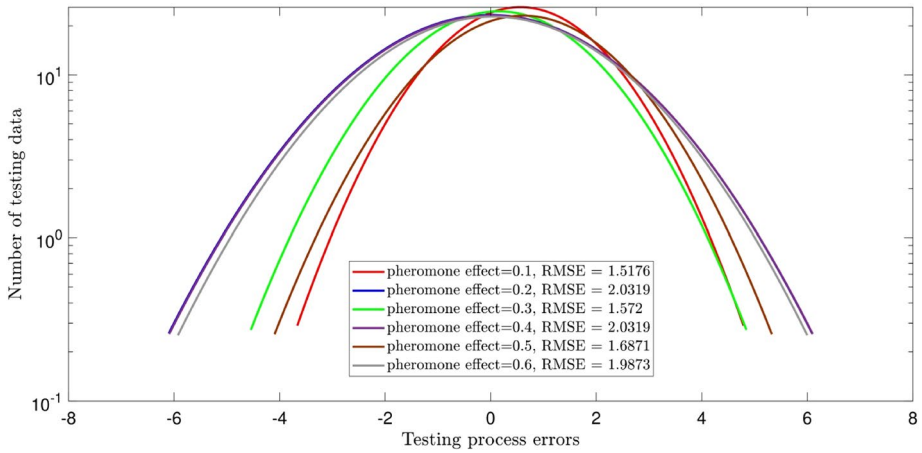

Figure 3. ACOFIS learning processes using three inputs and diversity of pheromone effect.

$$\begin{aligned} \tau_{ij} &\leftarrow \tau_{ij} + \sum_{k=1}^{n} \Delta\tau_{ij}^{k} + e\Delta\tau_{ij}^{bs}, \forall(i,j) \in L \\ \Delta\tau_{ij}^{bs} &= \begin{cases} \frac{1}{C^{bs}}, & if arc(i,j) belongs to T^{bs}; \\ 0, & otherwise; \end{cases} \end{aligned} \tag{15}$$

The rank-based version is another enhancement over ant system. Each ant deposits some pheromone decreasing by its rank. Moreover, the largest quantity of pheromone is always deposited by the best-ant-so-far during every iteration[38–40].

$$\tau_{ij} \leftarrow \tau_{ij} + \sum_{r=1}^{w-1} (w-r)\Delta\tau_{ij}^{r} + \Delta\tau_{ij}^{bs} \tag{16}$$

Fuzzy inference system (FIS). The FIS is utilized in the fields of optimization, control, classification and prediction in engineering sciences. Here, if–then rules are employed to design the FIS structure[41]. In this rule, the signals are multiplied based on the AND rule as the node function. For case, the ith rule function can be written as[41]:

$$w_i = \emptyset(X)\delta(Y)\sigma(NVF) \tag{17}$$

The firing strength value is determined for each rule, as following[16,41]:

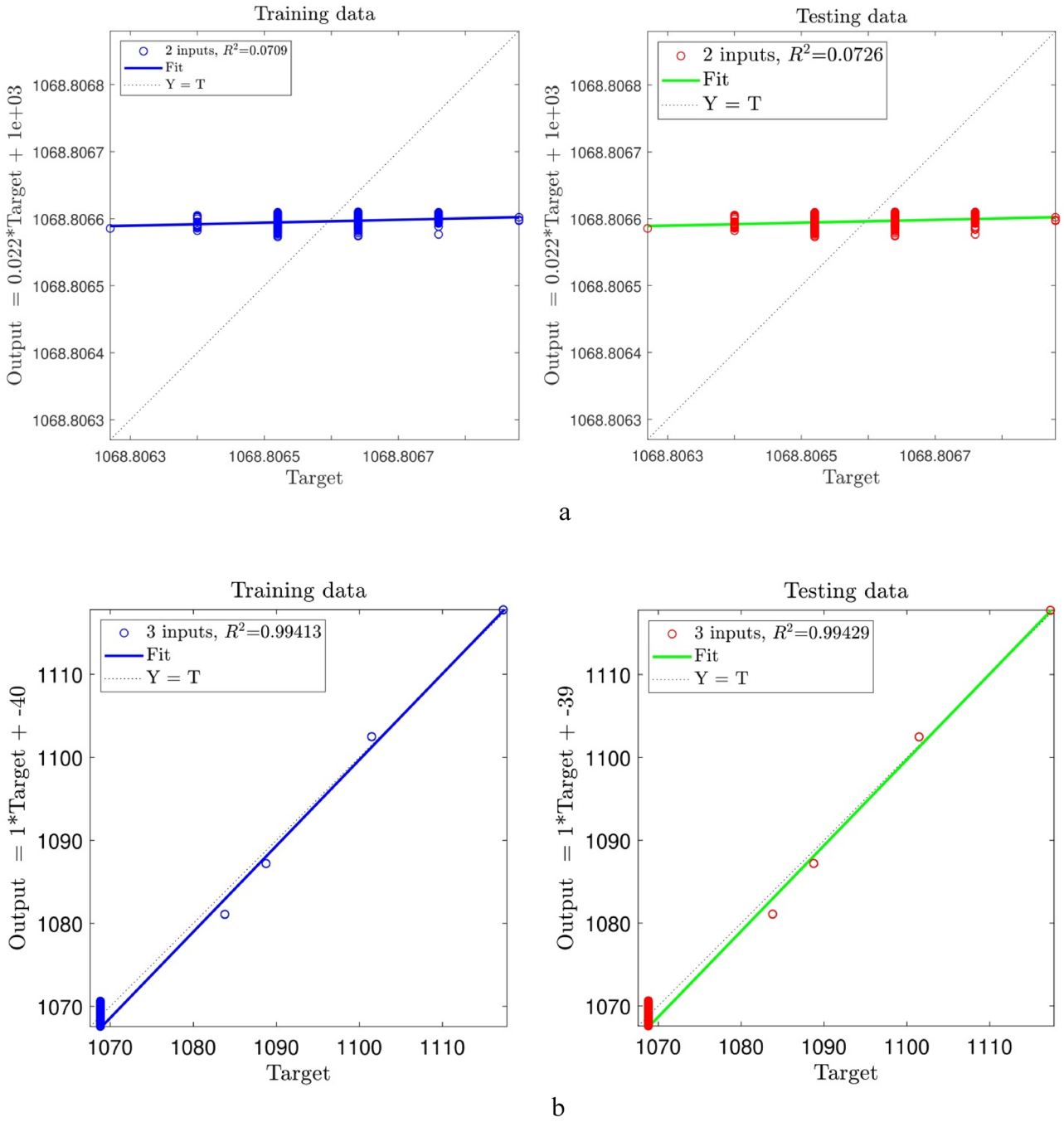

Figure 4. (**a**) Regression plot of the best of ACOFIS intelligence using two inputs in learning process. (**b**) Regression plot of the best of ACOFIS intelligence using three inputs in learning process.

$$\overline{w}_i = \frac{w_i}{\sum (w_i)} \tag{18}$$

where $\overline{w}_i$ is determined as normalized firing strengths. If–then rule developed by Takagi and Sugeno[41].

Consequently, the node function is:

$$\overline{w}_i f_i = \overline{w}_i \left(p_i X + q_i Y + r_i NVF + s_i\right) \tag{19}$$

Detailed descriptions of FIS can be found in our previous publications[16,42–46].

	ACOFIS for predicting pressure	ACOFIS for predicting temperature
CFD case study	Nanofluid turbulent flow in heated porous pipe	Nanofluid turbulent flow in heated porous pipe
AI method	Combination of ACO with FIS	Combination of ACO with FIS
Material of case study	Nanofluid (Al_2O_3)	Nanofluid (Al_2O_3)
Number of input in the best intelligence	3	3
Pheromone effect in the best intelligence (ACO parameter)	0.1	0.4
Changes in number of inputs was evaluated(FIS parameter)	2,3	3
Changes in pheromone effect was evaluated(ACO parameter)	0.1, 0.2, 0.3, 0.4, 0.5, 0.6	0.1, 0.2, 0.3, 0.4, 0.5, 0.6
The highest of correlation coefficient in testing process with 100% of data	0.994	0.968
P(%) percentage of used data in training process	77%	77%
Number of data	2 inputs (537) and 3 inputs (2685)	3 inputs (2685)
Number of iteration	115	115
Type of data clustering	FCM clustering	FCM clustering
Type of membership function	Guassmf	Guassmf
Number of MFs for each input	16	16
Number of rules (which is for hidden layer of FIS)	16	16
Number of membership functions (MFs) for output	16	16
ACOFIS input1	x-direction	x-direction
ACOFIS input2	y-direction	y-direction
ACOFIS input3	Nano particle Fraction = 0.5,0.8,1,1.5,2%	Nano particle Fraction = 0.5,0.8,1,1.5,2%
ACOFIS output	Pressure	Temperature

Table 3. ACOFIS setup for predicting pressure and temperature in the same setup.

Method	ACOFIS method	ANFIS method
Number of inputs	3	3
Percentage of data in training process	77	77
Number of iterations	115	115
Clustering Type	Fuzzy C-mean Clustering	Fuzzy C-mean Clustering
Exponent as FCM clustering parameter	2	2
Minimum Improvement as FCM clustering parameter	1.00E-05	1.00E-05
Correlation coefficient (R) in training process	0.997867326	0.99999993
Coefficient of determination (R^2) in training process	0.995739201	0.99999986
RMSE error in testing process	1.331970484	0.025145357
Correlation coefficient (R) in testing process	0.997857536	0.999998829
Coefficient of determination (R^2) in testing process	0.995719663	0.999997657
Learning process time (s)	198.0029725	212.5959348
Prediction process time (s)	0.1300083	0.519412

Table 4. Detail of ACOFIS and ANFIS setup and learning times.

Results and discussions

This study tries to develop a new artificial intelligence algorithm using the ant colony optimization, as a trainer, in a combination with the fuzzy inference system. The hybrid algorithm is then called ACOFIS. The ability of the developed algorithm is tested in the pressure and the temperature predictions of the Al_2O_3/H_2O NF in a porous tubular duct. Machine learning (ML) of the CFD results is employed in order to recognize the pattern of the flow characteristics. The pressure and temperature of the nanofluid on the cross-section plate at 0.3 m from the inlet are considered for such predictions in this study. Each trainer has its own parameters playing crucial roles in the accurate predictions of the data patterns extracted from the CFD computations. These parameters could be also changeable from one CFD case study to another. The pheromone effect is one of the important parameters of ant colony optimization. The effect of such parameters in the accurate prediction of CFD results

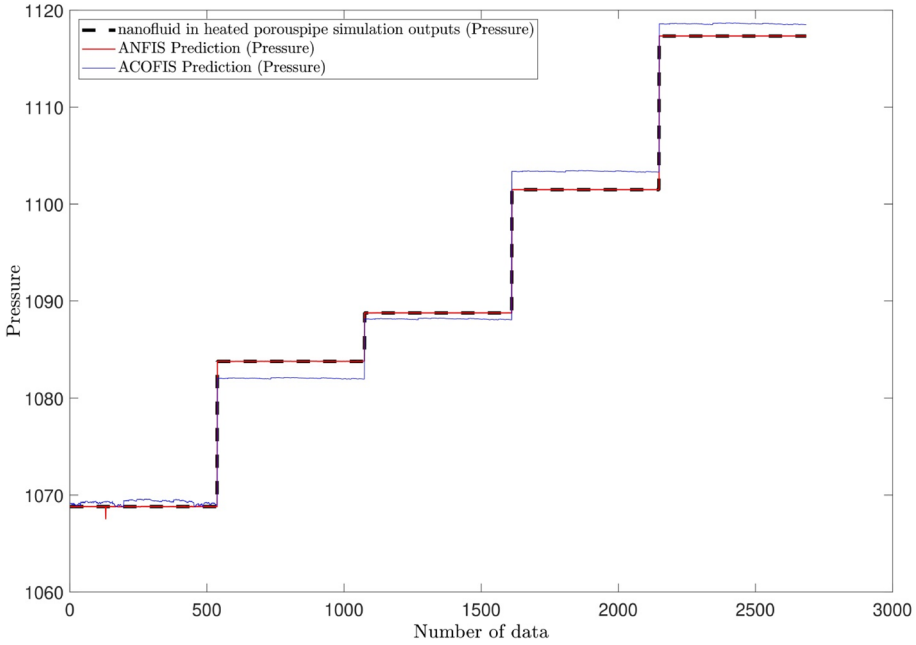

Figure 5. Comparison of pressure prediction with different AI methods.

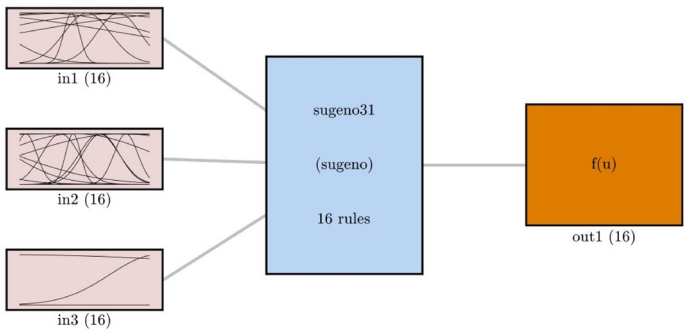

Figure 6. FIS structure in the best results.

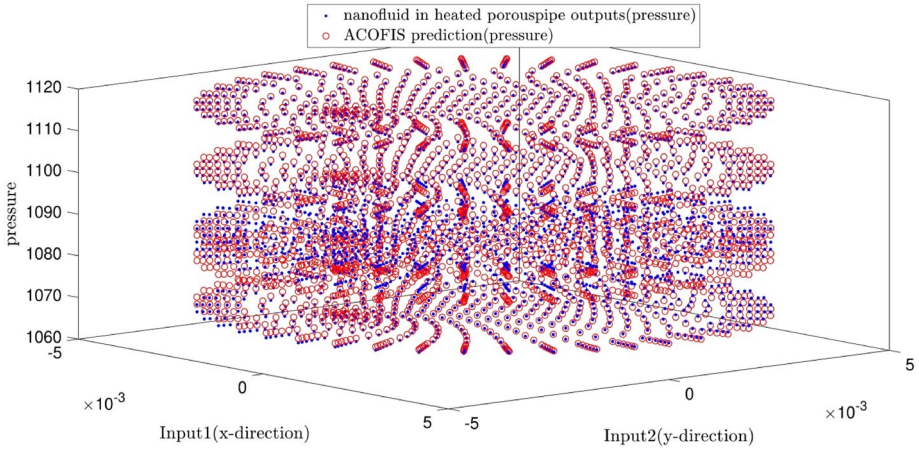

Figure 7. ACOFIS validation with comparison prediction data and CFD data.

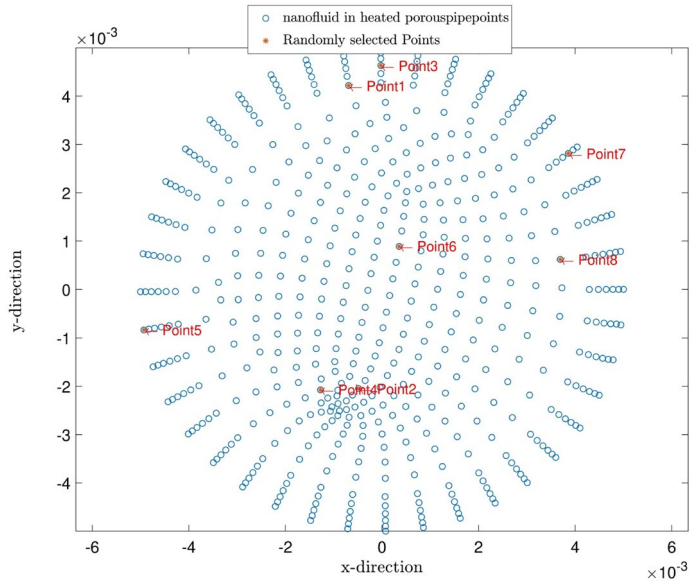

Figure 8. Random points for pattern recognition of pressure in different nanoparticle fractions.

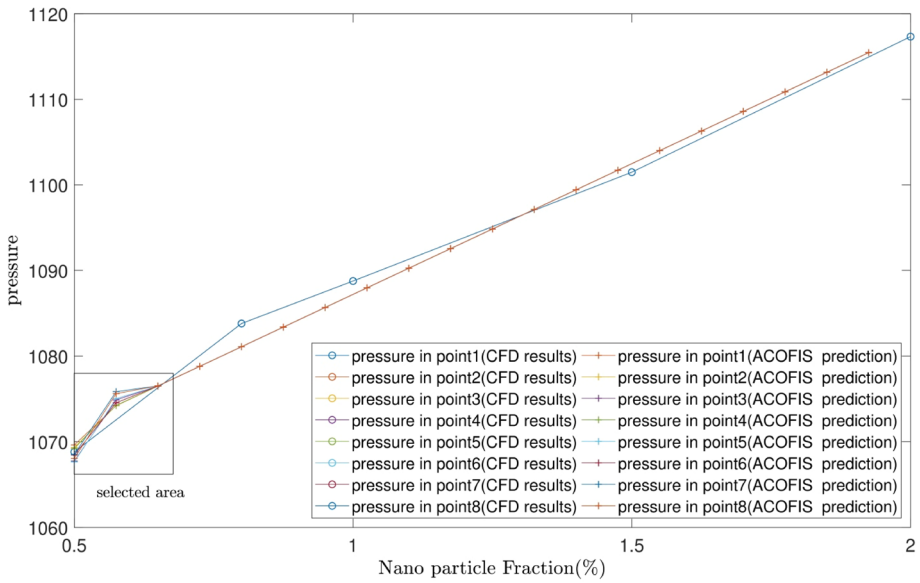

Figure 9. Pattern prediction of pressure in different Nano particle fractions.

is investigated in this study. The accuracy of the ACOFIS is checked with the CFD results and the predictions of the widely used artificial intelligence of ANFIS.

Figure 1 shows flowchart of using ACO as trainer in fuzzy inference system for learning the CFD results. As seen, the predicted pressures and temperatures are compared with the CFD calculations. The intelligence of model is checked by the root mean square error (RMSE) and the regression number (R). RMSE and the R values are recorded for different input numbers and pheromone effects. The lowest RMSE and the highest R means that the ACOFIS has achieved the best intelligence. At the best intelligence, for further validation, several nodes are selected randomly. The ACOFIS predicts nanofluid pressures and temperatures on the selected nodes for any values of the nanoparticles fraction.

Herein, the details of the tuning analysis of the ACOFIS are given just for the pressure prediction. Figure 2 shows the histogram error distribution graph for two inputs and different values of the pheromone effect. No change is seen by increasing the pheromone effect. Indeed, the error is distributed between ± 3, and the RMSE is around 9×10^{-5} for all values of the pheromone effect. Adding the nanoparticles volume fraction as the third input, the RMSE increases to the higher values (i.e. between 1.5 and 2) as illustrated in Fig. 3. According to Fig. 3, the error distribution and the RMSE are sensitive to the pheromone effect. The least RMSE (i.e. 1.5) is for the pheromone effect of 0.1 and the errors are distributed between ± 4. Although the RMSE value of 3 inputs

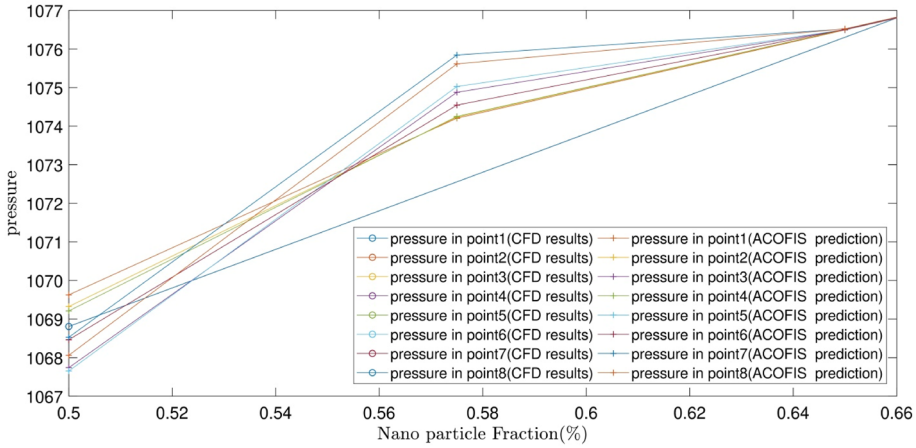

Figure 10. Selected area in Fig. 9.

is higher than that of 2 inputs, the ACOFIS reaches the best intelligence for the case when 3 inputs have been considered. This is shown in Fig. 4; the increase of input number from 2 to 3 leads to the increase of regression number from 0.07 to 0.99. Therefore, the RMSE only is not enough for intelligence determination. The RMSE increment by the number of inputs could be justified by the increase of data from 547 for 2 inputs to 2685 for 3 inputs. In fact, learning more data leads to more RMSE.

A similar analysis could be done for the best condition in prediction of temperature. A summary of this analysis and its results are given in Table 3. Unlike the pressure, the pheromone effect is equal to 0.4 at the best intelligence in prediction of temperature. This means that AI algorithms should be tuned for the prediction of each type of parameter.

For more validation, the predictions of the newly developed AI algorithm of ACOFIS are compared with the widely used algorithm of ANFIS. Table 4 explains this comparison. For similar iteration number, input number and clustering type, both methods achieve the highest values (around 1) of the correlation coefficient (R) and the coefficient of determination (R^2) in their predictions. The RMSE of ACOFIS (~ 1.3) is a little more than that of ANFIS (~ 0.03). This is shown in Fig. 5 where a comparison has been made between the ACOFIS and the ANFIS predictions of pressure for all learned data. The CFD results have been also shown as a benchmark. The ACOFIS predictions are close to the ANFIS and CFD results with a little deviation.

The learning time and prediction time of the ANFIS (212.6 s and 0.5 s respectively) are a little bit more than those of the ACOFIS (198 s and 0.1 s respectively). Although the total time difference is not that much (less than 15 s), this could be significant in actual large-scale cases. Totally, the summation of the learning and the prediction times take just a few minutes (less than 4 min). This means the AI algorithms could be so fast and as a result, need a little computational requirement in comparison with challenging and expensive CFD computations.

Figure 6 describes the number of membership functions (MFs) for each input, the number of rules, and the number of MFs for the output. All these numbers are equal to 16.

Figure 7 illustrates the predicted pressure of the nanofluid at different nanoparticles volume fractions by both CFD and ACOFIS models. The red points are the pressures of the nodes predicted by the ACOFIS, while the blue ones are the data simulated by the CFD. The ACOFIS predictions are the same as the CFD. Both methods show the increase of the pressure by nanoparticles volume fraction increment. 8 nodes on the cross-section plate are randomly selected (as shown in Fig. 8). Figure 8 illustrates the pressure prediction of the selected nodes for some other nanoparticle volume fractions. According to Figs. 9 and 10, there is good compatibility between the predicted pressures of both methods specifically for higher nanoparticle fractions (i.e. more than 0.66%).

All the above-mentioned procedures are repeated for the temperature predictions of the nanofluid at different volume fractions. Figure 11 illustrates the temperature contour of the nanofluid. According to Fig. 11a,b, the temperature predictions by the ACOFIS are compatible with the CFD. A curved surface is fitted to temperature predictions of the ACOFIS. This surface could give the temperature in any random location on the domain. For example, several nodes randomly selected from the domain, as shown in Fig. 12. The pattern of changing temperature in selected points by the nanoparticle fraction has been predicted and depicted in Fig. 13. This means there is no need for more CFD calculations for new nanoparticle fractions. The fast ACOFIS calculation could be replaced with the time-consuming method of CFD.

Conclusions

Although the CFD methods have a progressive trend in the precise prediction of the physical phenomena, there is not enough evidence for optimization of the CFD approach complexities. They might take more CPU time or require more computational hardware requirements especially in complex problems. So, another method is required for the CFD simplification. The machine learning (ML) of the artificial intelligence (AI) algorithms has shown the significant roles in finding the general patterns of the CFD results. In this case, the adaptive network (AN), as a data trainer, combining with the fuzzy inference system (FIS) has been commonly used. Each trainer has its own specific tuning parameters, and the accurate prediction of the AI algorithms are so dependent on

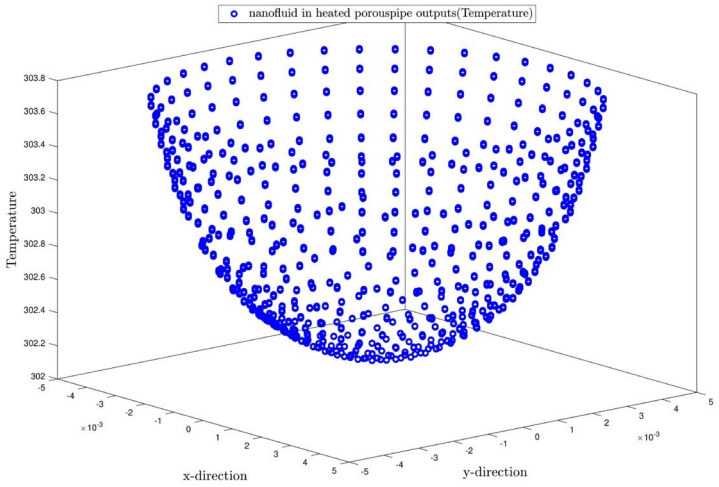

a

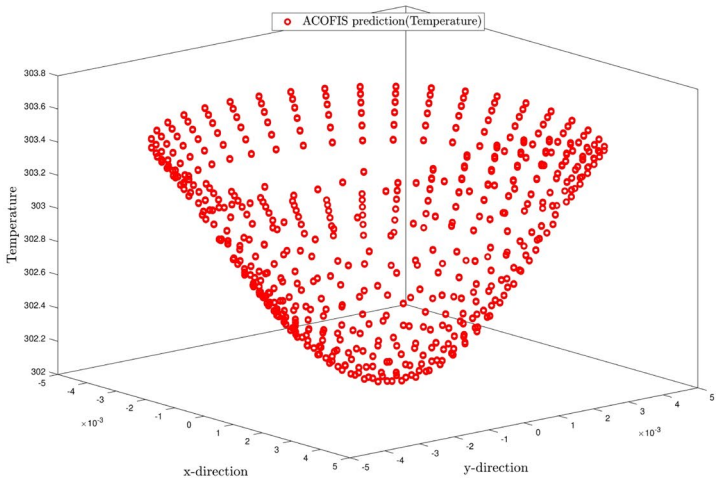

b

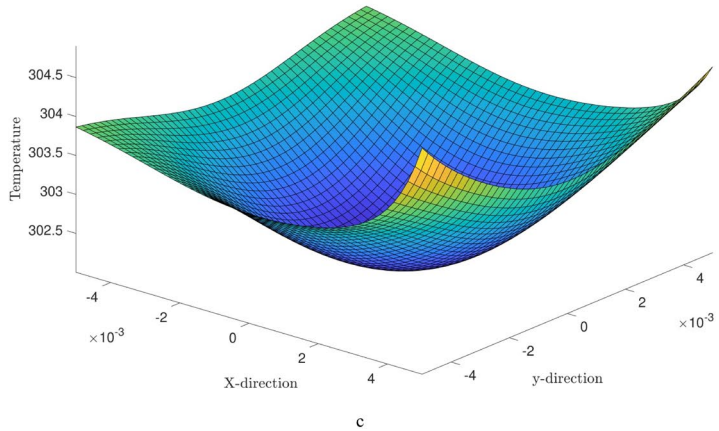

c

Figure 11. (**a**) CFD simulation results. (**b**) ACOFIS temperature prediction. (**c**) ACOFIS prediction surface for predicting temperature in different points.

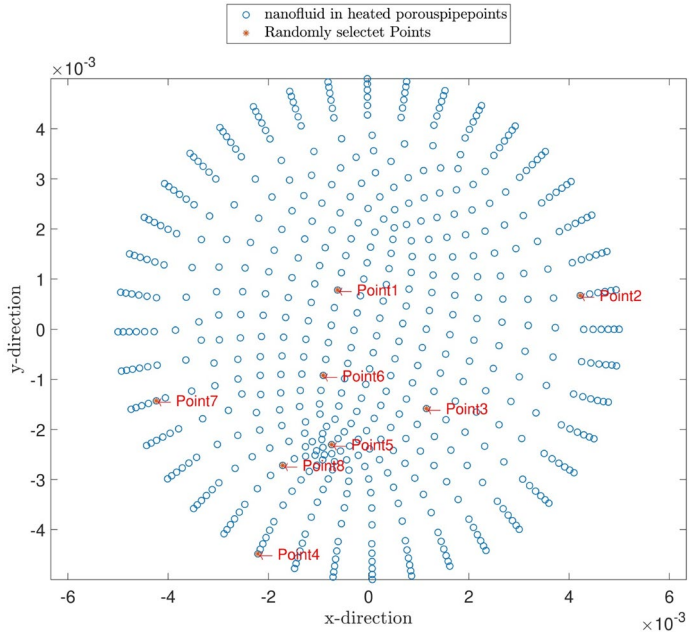

Figure 12. Random selected points for prediction of temperature in different nanoparticle fractions.

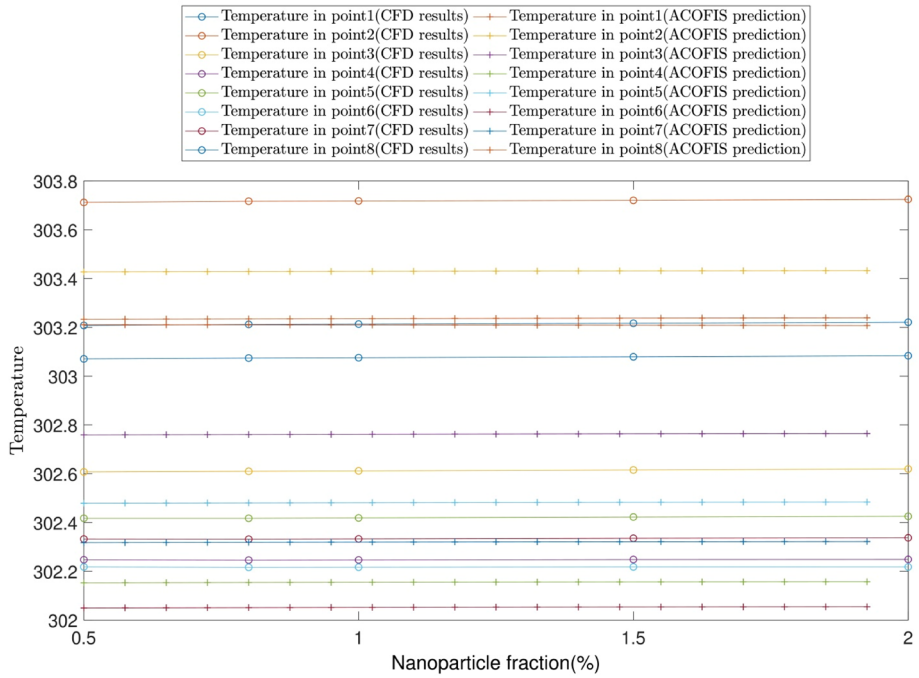

Figure 13. Pattern of predicted temperature in different nanoparticle fractions.

the proper selection of these parameters. But there are no investigations available for the efficiency comparison between the AN and the other trainers.

So, this study was aimed to develop the combination of the ant colony optimization (ACO) algorithm with the fuzzy inference system (ACOFIS) for learning the CFD results. This integration of the ACOFIS and the CFD was used for pressure and temperature predictions of Al_2O_3/water nanofluid flow in a heated porous pipe. Firstly, the case was simulated by the ANSYS-FLUENT CFD package. Considering the effect of the Brownian motion, User Defined Function (UDF) codes have been developed for effective conductivity and viscosity. The UDF codes were added to the ANSYS-FLUENT commercial CFD codes. Then the ACOFIS learned the CFD results including the pressure and the temperature of the nanofluid on the cross-section plate at z equal to 0.3 m. The intelligence of the ACOFIS was investigated for different input numbers and pheromone effects. For two inputs (i.e. x, and y

coordinates of the nodes), the ACOFIS learned the CFD results of the case for the nanoparticles volume fraction of 0.5. For this condition, the ACOFIS intelligence conditions were not met and the regression number was 0.07. However, increasing the nanoparticles volume fractions as the third input, the number of data increased from 547 to 2685 and as a result, the ACOFIS reached the intelligence with the R value of 0.98. Moreover, the testing different pheromone effect, the value of 0.1 showed the least of RMSE and the best intelligence. The validation test confirmed the high agreement between the CFD results and ACOFIS predictions. The ACOFIS also showed the ability of the accurate pressure and temperature predictions for any other nanoparticle fractions.

Comparing the ANFIS and the ACOFIS, it was shown that both methods could achieve the R and R^2 of 1 for 3 inputs and the same FIS parameters. The root mean square error of the ACOFIS (~ 1.3) was a little more than that of the ANFIS (~ 0.03), while the total process time of the ANFIS (~ 213 s) was a bit more than that of the ACOFIS (~ 198 s). Although the total time difference was not a lot (less than 15 s), this could increase significantly in real large-scale cases. Finally, it should be noted that the AI algorithms could be so quick prediction (less than 4 min).

This research area is at the beginning. It is recommended to continue the investigations on the other trainers such as neural network, genetic algorithm, bee algorithm, etc., and their tuning parameters for accurate prediction of fluid flow parameters in more complex CFD cases.

Received: 9 September 2020; Accepted: 11 December 2020
Published online: 08 January 2021

References

1. Hosseinzadeh, K., Moghaddam, M. E., Asadi, A., Mogharrebi, A. & Ganji, D. Effect of internal fins along with hybrid nano-particles on solid process in star shape triplex latent heat thermal energy storage system by numerical simulation. *Renew. Energy* (2020).
2. Mahanthesh, B., Mabood, F., Gireesha, B. & Gorla, R. Effects of chemical reaction and partial slip on the three-dimensional flow of a nanofluid impinging on an exponentially stretching surface. *Eur. Phys. J. Plus* **132**, 1–18 (2017).
3. Mahanthesh, B., Shashikumar, N. S. & Lorenzini, G. Heat transfer enhancement due to nanoparticles, magnetic field, thermal and exponential space-dependent heat source aspects in nanoliquid flow past a stretchable spinning disk. *J. Therm. Anal. Calorimetry* 1–9 (2020).
4. Aziz, A. & Khan, W. Natural convective boundary layer flow of a nanofluid past a convectively heated vertical plate. *Int. J. Therm. Sci.* **52**, 83–90 (2012).
5. Krauzina, M. T., Bozhko, A. A., Krauzin, P. V. & Suslov, S. A. The use of ferrofluids for heat removal: Advantage or disadvantage?. *J. Magn. Magn. Mater.* **431**, 241–244 (2017).
6. Bahiraei, M. & Hangi, M. Flow and heat transfer characteristics of magnetic nanofluids: a review. *J. Magn. Magn. Mater.* **374**, 125–138 (2015).
7. Liu, H., Animasaun, I., Shah, N. A., Koriko, O. & Mahanthesh, B. Further discussion on the significance of quartic autocatalysis on the dynamics of water conveying 47 nm alumina and 29 nm cupric nanoparticles. *Arab. J. Sci. Eng.* **45**, 5977–6004 (2020).
8. Azizifar, S., Ameri, M. & Behroyan, I. Subcooled flow boiling of water in a metal-foam tube: An experimental study. *Int. Commun. Heat Mass Transfer* **118**, 104897 (2020).
9. Azizifar, S., Ameri, M. & Behroyan, I. An experimental study of subcooled flow boiling of water in the horizontal and vertical direction of a metal-foam tube. *Thermal Sci. Eng. Progress* **20**, 100748 (2020).
10. Nazari, M., Baie, N. B., Ashouri, M., Shahmardan, M. & Tamayol, A. Unsteady heat transfer from a reservoir fluid by employing metal foam tube, helically tube and straight tube: a comparative experimental study. *Appl. Therm. Eng.* **111**, 39–48 (2017).
11. Mebarek-Oudina, F., Aissa, A., Mahanthesh, B. & Öztop, H. F. Heat transport of magnetized Newtonian nanoliquids in an annular space between porous vertical cylinders with discrete heat source. *Int. Commun. Heat Mass Transfer* **117**, 104737 (2020).
12. Saryazdi, A. B., Talebi, F., Armaghani, T. & Pop, I. Numerical study of forced convection flow and heat transfer of a nanofluid flowing inside a straight circular pipe filled with a saturated porous medium. *Eur. Phys. J. Plus* **131**, 78 (2016).
13. Marjani A, Babanezhad M, Shirazian S (2020) Application of adaptive network-based fuzzy inference system (ANFIS) in the numerical investigation of Cu/water nanofluid convective flow. Case Stud Therm Eng 22:100793
14. Wang H, Guo L, Chen K (2020) Theoretical and experimental advances on heat transfer and flow characteristics of metal foams. Sci China Technol Sci 63(5):705–718
15. Nguyen, Q., Behroyan, I., Rezakazemi, M. & Shirazian, S. Fluid velocity prediction inside bubble column reactor using ANFIS algorithm based on CFD input data. *Arab. J. Sci. Eng.* (2020).
16. Babanezhad, M., Nakhjiri, A. T. & Shirazian, S. Changes in the number of membership functions for predicting the gas volume fraction in two-phase flow using grid partition clustering of the ANFIS method. *ACS Omega* **5**, 16284–16291 (2020).
17. Zhou, J., Li, C., Arslan, C. A., Hasanipanah, M. & Amnieh, H. B. Performance evaluation of hybrid FFA-ANFIS and GA-ANFIS models to predict particle size distribution of a muck-pile after blasting. *Eng. Comput.* 1–10 (2019).
18. Xu, P., Babanezhad, M., Yarmand, H. & Marjani, A. Flow visualization and analysis of thermal distribution for the nanofluid by the integration of fuzzy c-means clustering ANFIS structure and CFD methods. *J. Vis.* 1–14 (2019).
19. Chin, R. J., Lai, S. H., Ibrahim, S., Jaafar, W. Z. W. & Elshafie, A. ANFIS-based model for predicting actual shear rate associated with wall slip phenomenon. *Soft Comput.* 1–11 (2019).
20. Cao, Y., Babanezhad, M., Rezakazemi, M. & Shirazian, S. Prediction of fluid pattern in a shear flow on intelligent neural nodes using ANFIS and LBM. *Neural Comput. Appl.* **32**, 13313–13321 (2019).
21. Pourtousi, M., Zeinali, M., Ganesan, P. & Sahu, J. Prediction of multiphase flow pattern inside a 3D bubble column reactor using a combination of CFD and ANFIS. *RSC Adv.* **5**, 85652–85672 (2015).
22. Pourtousi, M., Sahu, J., Ganesan, P., Shamshirband, S. & Redzwan, G. A combination of computational fluid dynamics (CFD) and adaptive neuro-fuzzy system (ANFIS) for prediction of the bubble column hydrodynamics. *Powder Technol.* **274**, 466–481 (2015).
23. Behroyan, I., Ganesan, P., He, S. & Sivasankaran, S. Turbulent forced convection of Cu–water nanofluid: CFD model comparison. *Int. Commun. Heat Mass Transfer* **67**, 163–172 (2015).
24. Ameri, M., Amani, M. & Amani, P. Thermal performance of nanofluids in metal foam tube: Thermal dispersion model incorporating heterogeneous distribution of nanoparticles. *Adv. Powder Technol.* **28**, 2747–2755 (2017).
25. Sedighi, A. A., Deldoost, Z. & Karambasti, B. M. Flow and heat transfer of nanofluid in a channel partially filled with porous media considering turbulence effect in pores. *Can. J. Phys.* **98**, 297–302 (2020).
26. Shih, T. M. *Numerical Heat Transfer*. (CRC Press, 1984).
27. Mohammed, H. I. & Giddings, D. Multiphase flow and boiling heat transfer modelling of nanofluids in horizontal tubes embedded in a metal foam. *Int. J. Therm. Sci.* **146**, 106099 (2019).
28. Xu, H., Qu, Z. & Tao, W. Thermal transport analysis in parallel-plate channel filled with open-celled metallic foams. *Int. Commun. Heat Mass Transfer* **38**, 868–873 (2011).

29. Zhao, C., Kim, T., Lu, T. & Hodson, H. *Thermal transport phenomena in porvair metal foams and sintered beds* (University of Cambridge, Final Report, 2001).
30. Nield, D. A. & Bejan, A. in *Convection in porous media* 37–55 (Springer, 2017).
31. Chon, C. H., Kihm, K. D., Lee, S. P. & Choi, S. U. Empirical correlation finding the role of temperature and particle size for nanofluid (Al2O3) thermal conductivity enhancement. *Appl. Phys. Lett.* **87**, 153107 (2005).
32. Masoumi, N., Sohrabi, N. & Behzadmehr, A. A new model for calculating the effective viscosity of nanofluids. *J. Phys. D Appl. Phys.* **42**, 055501 (2009).
33. Ajeel, R. K., Salim, W.-I. & Hasnan, K. Experimental and numerical investigations of convection heat transfer in corrugated channels using alumina nanofluid under a turbulent flow regime. *Chem. Eng. Res. Des.* **148**, 202–217 (2019).
34. Ganesan, P., Behroyan, I., He, S., Sivasankaran, S. & Sandaran, S. C. Turbulent forced convection of Cu–water nanofluid in a heated tube: Improvement of the two-phase model. *Numer. Heat Transfer, Part A Appl.* **69**, 401–420 (2016).
35. Fotukian, S. & Esfahany, M. N. Experimental investigation of turbulent convective heat transfer of dilute γ-Al2O3/water nanofluid inside a circular tube. *Int. J. Heat Fluid Flow* **31**, 606–612 (2010).
36. Li, Y. & Li, W. Adaptive ant colony optimization algorithm based on information entropy: Foundation and application. *Fund. Inf.* **77**, 229–242 (2007).
37. Reinhelt, G. {TSPLIB}: a library of sample instances for the TSP (and related problems) from various sources and of various types. http://comopt.ifi.uniheidelberg.de/software/TSPLIB95 (2014).
38. Castillo, O., Neyoy, H., Soria, J., García, M. & Valdez, F. Dynamic fuzzy logic parameter tuning for ACO and its application in the fuzzy logic control of an autonomous mobile robot. *Int. J. Adv. Rob. Syst.* **10**, 51. https://doi.org/10.5772/54883 (2013).
39. Castillo, O., Melin, P. & Kacprzyk, J. *Recent advances on hybrid intelligent systems*. (Springer, 2013).
40. Dorigo, M., Birattari, M. & Stutzle, T. Ant colony optimization. *IEEE Comput. Intell. Mag.* **1**, 28–39 (2006).
41. Takagi, T. & Sugeno, M. Fuzzy identification of systems and its applications to modeling and control. *IEEE Trans. Syst. Man Cybern.* 116–132 (1985).
42. Pishnamazi, M. *et al.* ANFIS grid partition framework with difference between two sigmoidal membership functions structure for validation of nanofluid flow. *Sci. Rep.* **10**, 1–11 (2020).
43. Babanezhad, M., Taghvaie Nakhjiri, A., Rezakazemi, M. & Shirazian, S. Developing Intelligent Algorithm as a Machine Learning Overview over the Big Data Generated by Euler–Euler Method To Simulate Bubble Column Reactor Hydrodynamics. *ACS Omega* (2020).
44. Babanezhad, M., Pishnamazi, M., Marjani, A. & Shirazian, S. Bubbly flow prediction with randomized neural cells artificial learning and fuzzy systems based on k–ε turbulence and Eulerian model data set. *Sci. Rep.* **10**, 1–12 (2020).
45. Babanezhad, M., Nakhjiri, A. T., Marjani, A. & Shirazian, S. Pattern recognition of the fluid flow in a 3D domain by combination of Lattice Boltzmann and ANFIS methods. *Sci. Rep.* **10**, 1–13 (2020).
46. Babanezhad, M. *et al.* Prediction of turbulence eddy dissipation of water flow in a heated metal foam tube. *Sci. Rep.* **10**, 1–12 (2020).

Acknowledgements

This work was supported by the Government of the Russian Federation (Act 211, contract 02.A03.21.0011) and by the Ministry of Science and Higher Education of Russia (Grant FENU-2020-0019).

Author contributions

M.B.: simulations, writing-draft; I.B: software, modeling, revision; A.M.: supervision, validation; S.S.: funding acquisition, modeling, writing-review, revision.

Competing interests

The authors declare no competing interests.

Additional information

Correspondence and requests for materials should be addressed to A.M.

Reprints and permissions information is available at www.nature.com/reprints.

Publisher's note Springer Nature remains neutral with regard to jurisdictional claims in published maps and institutional affiliations.